

# A Practical Solution for SAR Despeckling With Adversarial Learning Generated Speckled-to-Speckled Images

Ye Yuan, *Student Member, IEEE*, Jian Guan, *Member, IEEE*, Pengming Feng, *Member, IEEE*, and Yanxia Wu

**Abstract**—In this letter, we aim to address a synthetic aperture radar (SAR) despeckling problem with the necessity of neither clean (speckle-free) SAR images nor independent speckled image pairs from the same scene, and a practical solution for SAR despeckling (PSD) is proposed. First, an adversarial learning framework is designed to generate speckled-to-speckled (S2S) image pairs from the same scene in the situation where only single speckled SAR images are available. Then, the S2S SAR image pairs are employed to train a modified despeckling Nested-UNet model using the Noise2Noise (N2N) strategy. Moreover, an iterative version of the PSD method (PSDi) is also presented. Experiments are conducted on both synthetic speckled and real SAR data to demonstrate the superiority of the proposed methods compared with several state-of-the-art methods. The results show that our methods can reach a good tradeoff between feature preservation and speckle suppression.

**Index Terms**—Adversarial learning, image despeckling, Nested-UNet, Noise2Noise (N2N), synthetic aperture radar (SAR).

## I. INTRODUCTION

SYNTHETIC aperture radar (SAR) images are usually corrupted with speckle noise, which leads to the degradation of image quality and affects the performance in various applications of remote sensing [1], e.g., classification [2] and change detection [3]. Several methods have been proposed to mitigate the speckle in SAR images, including filtering methods [4], [5], wavelet shrinkage [6], [7], variational models [8]–[10], and SAR block-matching 3-D algorithm (SAR-BM3D) [11]. However, these methods sometimes fail to preserve sharp features such as edges or contain block artifacts in the despeckled images [12].

Recently, convolutional neural network (CNN)-based supervised learning has been employed for SAR despeckling

and achieved remarkable despeckling performance [13]–[16], which can reduce speckle noise by learning relationships between speckled and clean ground truth images with CNN models. However, there are few clean SAR images in practical applications. Hence, speckle-free optical images with the single channel are usually employed as the clean ground truth for SAR image despeckling, and synthetic speckled images can be obtained by adding speckle noise to original images. Then, such speckled-to-clean image pairs can be used as training data in CNN despeckling models. However, because of the differences in imaging mechanism and image features of SAR and optical images, i.e., gray-level distribution and spatial correlation [17], it is not the optimal solution to achieve SAR image despeckling by directly employing the aforementioned CNN models, which are trained on optical images using supervised learning.

More recently, the Noise2Noise (N2N) [18] strategy has shown its ability for image denoising without using any clean ground-truth images. By employing the N2N strategy, the CNN model can still achieve high denoising performance (e.g., zero-mean distribution noise) with mean square error (MSE) loss, as long as two independent noisy images from the same underlying clean image are available. This provides the possibility for SAR image despeckling without using clean ground-truth images. However, to acquire two independent speckled SAR images from the same scene is quite difficult. Hence, it is still impossible to solve the SAR image despeckling problem by merely employing the N2N strategy, as only single speckled SAR images are available.

In this letter, we introduce a practical despeckling solution for SAR image in the situation of only single speckled images are available, namely, a practical solution for SAR despeckling (PSD). Our contributions are summarized as follows.

- 1) To generate speckled-to-speckled (S2S) SAR image pairs, an adversarial learning framework that consists of two generators and a discriminator is presented, which are trained by an alternating optimization strategy.
- 2) By using the obtained S2S SAR image pairs, an advanced Nested-UNet model [19] is trained to achieve despeckling with the N2N strategy. In addition, an iterative version of the PSD method (PSDi) is proposed, which can further improve the despeckling performance.
- 3) Visual and quantitative experiments conducted on synthetic speckled and real SAR data show that the

This work was supported in part by the Fundamental Research Funds for the Central Universities under Grant 3072020CFT0602, in part by the Open Research Fund of State Key Laboratory of Space Ground Integrated Information Technology under Grant\_2018\_SGIIT\_KFJJ\_AI\_01, and in part by the National Natural Science Foundation of China under Grant 61806018. (Corresponding author: Jian Guan.)

Ye Yuan, Jian Guan, and Yanxia Wu are with the College of Computer Science and Technology, Harbin Engineering University, Harbin 150001, China (e-mails: yuanye@hrbeu.edu.cn, j.guan@hrbeu.edu.cn, wuyanxia@hrbeu.edu.cn).

Pengming Feng is with the State Key Laboratory of Space-Ground Integrated Information Technology, China Academy of Space Technology, Beijing 100086, China (e-mail: p.feng.cn@outlook.com).

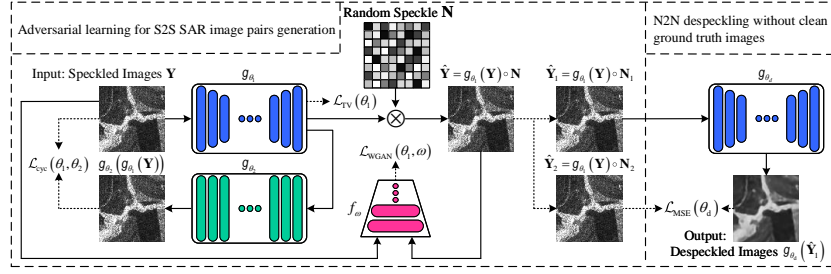


Fig. 1. Overall flowchart of the proposed PSD method. (Left) Adversarial learning for S2S SAR image pairs generation: two generators  $g_{\theta_1}$  and  $g_{\theta_2}$  and a discriminator  $f_{\omega}$  are trained by using the adversarial loss  $\mathcal{L}_{WGAN}$ , the backward cycle consistency loss  $\mathcal{L}_{cyc}$ , and the TV loss  $\mathcal{L}_{TV}$ . (Right) N2N despeckling without clean ground truth images: the despeckling model  $g_{\theta_d}$  is trained by using the MSE loss  $\mathcal{L}_{MSE}$ .  $\otimes$  denotes adding multiplicative speckle noise according to (1) and (2).

proposed methods notably suppress speckle noise with better preserving features, which outperform several state-of-the-art despeckling methods.

## II. METHODOLOGY

In this section, we present implementation details of the proposed PSD method as shown in Fig. 1, which consists of two parts: 1) adversarial learning framework for S2S SAR image pairs generation and its loss functions for optimization and 2) N2N despeckling strategy without using any clean ground-truth images and the despeckling network architecture of the modified Nested-UNet.

### A. SAR Speckle Noise Model

Let  $\mathbf{Y} \in \mathbb{R}^{W \times H}$  be the observed SAR image with the size of  $W \times H$ ,  $\mathbf{X} \in \mathbb{R}^{W \times H}$  be the underlying (despeckled) clean image, and  $\mathbf{N} \in \mathbb{R}^{W \times H}$  be the speckle noise. Then  $\mathbf{Y}$  can be obtained by the following multiplicative model [14]:

$$\mathbf{Y} = \mathbf{X} \circ \mathbf{N} \quad (1)$$

where  $\circ$  denotes the Hadamard product (i.e., entrywise product) of two matrices and  $\mathbf{N}$  is assumed to follow a gamma distribution with unit mean. The probability density function of  $\mathbf{N}$  can be written as [14]:

$$p(\mathbf{N}) = \frac{L^L \mathbf{N}^{L-1} e^{-L\mathbf{N}}}{\Gamma(L)}. \quad (2)$$

Here,  $\Gamma(\cdot)$  denotes the gamma function and  $L$  is the number of looks in SAR imaging process, where a smaller  $L$  indicates stronger speckle. In this work, the approach of adding speckle noise is following the scheme in (1) and (2). The aim of despeckling is to estimate  $\mathbf{X}$  from the observed image  $\mathbf{Y}$ . Based on the established speckle noise model in (1) and (2), our proposed approach in Section II-B can be used to generate S2S SAR image pairs from the same scenario.

### B. Adversarial Learning for S2S SAR Image Pairs Generation

To generate S2S SAR image pairs, we introduce an adversarial learning framework, which consists of two generators  $g_{\theta_1}$  and  $g_{\theta_2}$ , and a discriminator  $f_{\omega}$ , as shown in Fig. 1 (left).  $\theta_1$ ,  $\theta_2$  and  $\omega$  denote the parameters (i.e., weights and biases)

of  $g_{\theta_1}$ ,  $g_{\theta_2}$  and  $f_{\omega}$ , respectively.  $g_{\theta_1}$  is used to generate the “fake” speckled SAR images  $\hat{\mathbf{Y}}$ , expressed as follows:

$$\hat{\mathbf{Y}} = g_{\theta_1}(\mathbf{Y}) \circ \mathbf{N}. \quad (3)$$

The network architecture of  $g_{\theta_1}$  is the same as the despeckling model  $g_{\theta_d}$ , which will be described in Section II-C. Also, the discriminator  $f_{\omega}$  determines the distance between the distribution of the “fake” speckled SAR images and the distribution of the input speckled images, and its network architecture is designed as suggested in [20].  $g_{\theta_1}$  and  $f_{\omega}$  are trained by the adversarial loss of Wasserstein generative adversarial networks (WGANs) [21]  $\mathcal{L}_{WGAN}$ , which can be formulated as

$$\mathcal{L}_{WGAN}(\theta_1, \omega) = \mathbb{E}[f_{\omega}(\mathbf{Y})] - \mathbb{E}[f_{\omega}(g_{\theta_1}(\mathbf{Y}) \circ \mathbf{N})], \quad (4)$$

where  $\mathbb{E}$  denotes the expectation operator.

To make  $g_{\theta_1}$  change speckle distribution while preserving the basic edge features of the original SAR image,  $g_{\theta_2}$  is used to bring the output of  $g_{\theta_1}$  back to the original SAR image, namely,  $\mathbf{Y} \rightarrow g_{\theta_1}(\mathbf{Y}) \rightarrow g_{\theta_2}(g_{\theta_1}(\mathbf{Y})) \approx \mathbf{Y}$ . We design the network architecture of  $g_{\theta_2}$  following the denoising CNN (DnCNN) [22].  $g_{\theta_1}$  and  $g_{\theta_2}$  are trained by the backward cycle consistency loss  $\mathcal{L}_{cyc}$  following [20] and [23], denoted as

$$\mathcal{L}_{cyc}(\theta_1, \theta_2) = \mathbb{E}[\|\mathbf{Y} - g_{\theta_2}(g_{\theta_1}(\mathbf{Y}))\|_1]. \quad (5)$$

In addition, to smooth the output of  $g_{\theta_1}$ , the generator  $g_{\theta_1}$  is also trained by the total variation (TV) loss  $\mathcal{L}_{TV}$ , which is defined as

$$\mathcal{L}_{TV}(\theta_1) = \sum_{w=1}^{W-1} \sum_{h=1}^{H-1} (|g_{\theta_1}(\mathbf{Y})_{w+1,h} - g_{\theta_1}(\mathbf{Y})_{w,h}|^2 + |g_{\theta_1}(\mathbf{Y})_{w,h+1} - g_{\theta_1}(\mathbf{Y})_{w,h}|^2)^{1/2} \quad (6)$$

where  $g_{\theta_1}(\mathbf{Y})_{w,h}$  is the pixel value in  $g_{\theta_1}(\mathbf{Y})$  and  $\mathcal{L}_{TV}$  can reduce the difference of adjacent pixel values in the despeckled images  $g_{\theta_1}(\mathbf{Y})$ .

With the defined loss functions, an alternating optimization strategy is applied to optimize  $g_{\theta_1}$ ,  $g_{\theta_2}$ , and  $f_{\omega}$ , which can be described as an adversarial min-max problem, expressed as

$$\min_{\theta_1, \theta_2} \max_{\omega} [\mathcal{L}_{WGAN}(\theta_1, \omega) + \mathcal{L}_{cyc}(\theta_1, \theta_2) + \alpha \mathcal{L}_{TV}(\theta_1)] \quad (7)$$

where  $\alpha$  is the predefined weight for  $\mathcal{L}_{TV}$ . To prevent  $g_{\theta_1}(\mathbf{Y})$  from being oversmooth,  $\alpha$  should be far less than 1 [14]. After reaching a steady state through adversarial learning, i.e., until

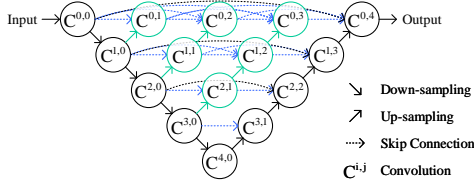


Fig. 2. Network architecture of Nested-UNet.

the discriminator  $f_\omega$  cannot distinguish the “fake” speckled SAR images  $g_{\theta_1}(\mathbf{Y}) \circ \mathbf{N}$  from the input speckled images  $\mathbf{Y}$ , then we can obtain the S2S SAR image pairs  $(\hat{\mathbf{Y}}_1, \hat{\mathbf{Y}}_2)$  from the same scene in the situation when only single speckled SAR images are available, which can be expressed as follows:

$$(\hat{\mathbf{Y}}_1, \hat{\mathbf{Y}}_2) = (g_{\theta_1}(\mathbf{Y}) \circ \mathbf{N}_1, g_{\theta_1}(\mathbf{Y}) \circ \mathbf{N}_2) \quad (8)$$

where  $\mathbf{N}_1$  and  $\mathbf{N}_2$  are two independent speckle matrices with the same number of looks  $L$ .

### C. N2N Despeckling Without Clean Ground-truth Images

After obtaining the S2S SAR image pairs  $(\hat{\mathbf{Y}}_1, \hat{\mathbf{Y}}_2)$ , we can employ the N2N strategy [18] to train the despeckling model  $g_{\theta_d}$  without using any clean ground truth images. Here, MSE loss is used to optimize  $g_{\theta_d}$ , which is formulated as

$$\mathcal{L}_{\text{MSE}}(\theta_d) = \|\hat{\mathbf{Y}}_2 - g_{\theta_d}(\hat{\mathbf{Y}}_1)\|_2 \quad (9)$$

where  $\theta_d$  denotes the parameters (i.e., weights and biases) of  $g_{\theta_d}$ . Due to the characteristic of speckle noise, as expressed in (1) and (2), the expected value of speckled image is the same as that of underlying despeckled image, which is expressed as follows:

$$\mathbb{E}[\hat{\mathbf{Y}}] = \mathbb{E}[g_{\theta_1}(\mathbf{Y}) \circ \mathbf{N}] = \mathbb{E}[g_{\theta_1}(\mathbf{Y})] \approx \mathbb{E}[\mathbf{X}]. \quad (10)$$

Hence, the minimum of  $\mathcal{L}_{\text{MSE}}$  can be found at the expectation of speckled images. This is particularly true when  $g_{\theta_d}$  is trained on a large data set. Therefore, we can generate despeckled images by using  $g_{\theta_d}$  without clean ground truth images.

A modified Nested-UNet [19] is adopted as the despeckling model  $g_{\theta_d}$ , as shown in Fig. 2. Nested-UNet is chosen because of its advantage in improving the gradients flow throughout the network by its convolution layers on skip pathways and dense skip connections on skip pathways. The original Nested-UNet is polished to be more effective for SAR image despeckling by removing batch normalization layers of each convolutional block, which has been proven in other image processing tasks, e.g., image super-resolution [24].

Except for the above PSD method, we also propose an iterative version of PSD method, named PSDi. For PSD method, the despeckling network is trained by using the generative S2S SAR image pairs  $(\hat{\mathbf{Y}}_1, \hat{\mathbf{Y}}_2)$ , and hence, their quality will affect the despeckling performance. The quality of the image pairs  $(\hat{\mathbf{Y}}_1, \hat{\mathbf{Y}}_2)$  can be described as how close is the distribution of  $(\hat{\mathbf{Y}}_1, \hat{\mathbf{Y}}_2)$  to that of the real speckled SAR image  $\mathbf{Y}$ . According to (1) and (8), we know  $(\hat{\mathbf{Y}}_1, \hat{\mathbf{Y}}_2)$  are generated by using  $g_{\theta_1}$ , and their quality is decided by the despeckling ability of  $g_{\theta_1}$ . However, the despeckling ability of

TABLE I  
PERFORMANCE COMPARISON IN TERMS OF PSNR AND SSIM ON SYNTHETIC SPECKLED DATA

The number of looks	PSNR			SSIM		
	1	4	16	1	4	16
Speckled Input	11.08	15.17	20.73	0.0519	0.1261	0.3052
Chen2014	13.64	13.27	-	0.4212	0.1651	-
SAR-BM3D	16.99	19.88	22.24	0.1799	0.2525	0.3604
SAR-DRN	25.25	28.39	29.77	0.5831	0.7143	0.8061
Ma2019	25.29	28.43	29.98	0.6237	0.7290	0.8059
PSD	25.47	28.45	<b>30.04</b>	0.7023	0.7571	0.8200
PSDi	<b>25.67</b>	<b>28.67</b>	29.92	<b>0.7196</b>	<b>0.7763</b>	<b>0.8284</b>

$g_{\theta_1}$  is not decent, as there are no available ground-truth (clean or speckled) images, whereas  $g_{\theta_d}$  can provide more powerful despeckling ability with ground-truth (speckled) images. Thus, to improve the quality of generative S2S SAR image pairs, we replace  $g_{\theta_1}$  with  $g_{\theta_d}$  in (8) and obtain the new S2S image pairs as follows:

$$(\tilde{\mathbf{Y}}_1, \tilde{\mathbf{Y}}_2) = (g_{\theta_d}(\mathbf{Y}) \circ \mathbf{N}_1, g_{\theta_d}(\mathbf{Y}) \circ \mathbf{N}_2). \quad (11)$$

With the new S2S image pairs, a more effective despeckling model  $g_{\theta_{di}}$  can be obtained by using N2N strategy again. Thereby, we can complete the training process of the despeckling model with only single speckled SAR images.

## III. EXPERIMENTS AND RESULTS

### A. Experimental Setup

In this work,  $2.2 \times 10^4$  one-look SAR image patches (cropped to  $96 \times 96$  pixels) obtained from the Sentinel-1 are used to train the proposed networks. In the training process of the adversarial learning (see Section II-B), to keep the noise level in the original one-look SAR images  $\mathbf{Y}$  consistent with that in the generated speckled images  $\hat{\mathbf{Y}}$ , the number of looks  $L$  for each generated speckled image is set to be 1. In the training process of the N2N despeckling (see Section II-C), to make the network available to different speckle levels, the number of looks  $L$  for  $(\hat{\mathbf{Y}}_1, \hat{\mathbf{Y}}_2)$  and  $(\tilde{\mathbf{Y}}_1, \tilde{\mathbf{Y}}_2)$  is randomly set to be 1, 2, 4, 8 and 16. The predefined weight  $\alpha$  is set to be 0.1. The networks  $g_{\theta_1}$ ,  $g_{\theta_2}$ ,  $g_{\theta_d}$ , and  $g_{\theta_{di}}$  are trained using the Adam optimizer with  $\beta_1 = 0.9$ ,  $\beta_2 = 0.999$ , and  $\epsilon = 10^{-8}$ , where the learning rates are all initialized as  $10^{-4}$  and reduced by half with each eight epochs. The network  $f_\omega$  is trained using the RMSProp optimizer with an initial learning rate of  $5 \times 10^{-5}$ . Following [21], the clipping value is set as 0.02, and the critic iteration is 5. The training process is set to have 16 epochs with mini-batch size 16 in both adversarial learning and N2N despeckling. PyTorch is employed to train the proposed methods with an Intel Xeon E5 CPU and an Nvidia 2080Ti GPU. The total training costs around 9 h 30 min.

To verify despeckling effectiveness, the proposed PSD ( $g_{\theta_d}$ ) and PSDi ( $g_{\theta_{di}}$ ) are compared with several state-of-the-art methods, i.e., variational-based Chen2014 [10], nonlocal-based SAR-BM3D [11], and SAR despeckling method with dilated residual network (SAR-DRN) [15] and Ma2019 [16]. Here, though Chen2014 and SAR-BM3D do not need any

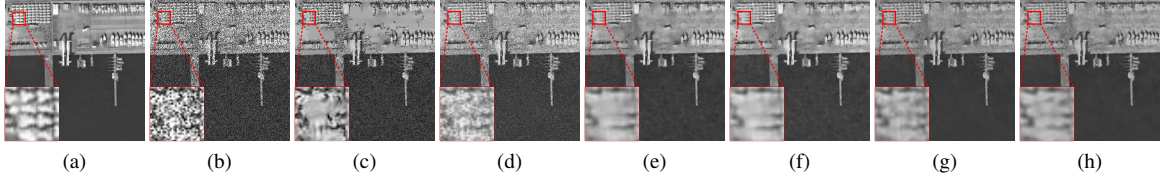


Fig. 3. Illustration of despeckling results on synthetic speckled image corrupted by four-look speckle. (a) Clean reference. (b) Speckled. (c) Chen2014. (d) SAR-BM3D. (e) SAR-DRN. (f) Ma2019. (g) PSD. (h) PSDi.

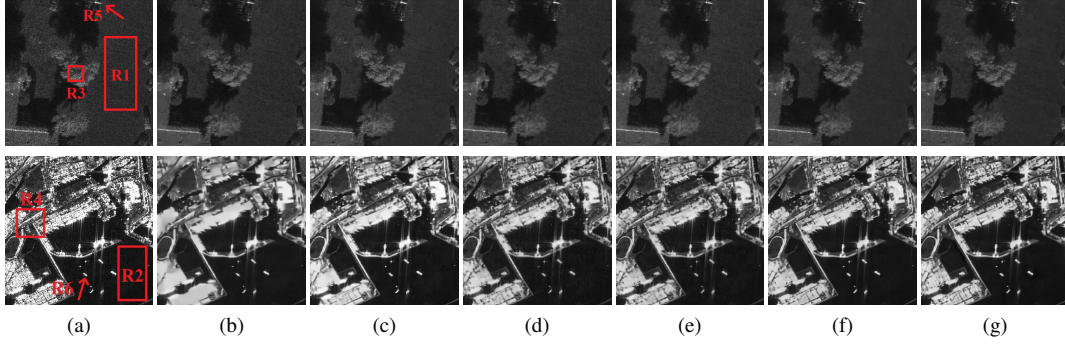


Fig. 4. (Top) Illustration of despeckling results on a three-look miniSAR image and (Bottom) a one-look Sentinel-1 SAR image. As identified by the red boxes and arrows, two homogeneous regions (R1 and R2) are employed to calculate ENL and MoR, two edge-feature regions (R3 and R4) are employed to calculate EPD-ROA, and two-point target regions (R5 and R6) are employed to calculate TCR. (a) Original image. (b) Chen2014. (c) SAR-BM3D. (d) SAR-DRN. (e) Ma2019. (f) PSD. (g) PSDi.

additional training, they have to know the number of looks  $L$ , whereas SAR-DRN and Ma2019 need clean ground truth images for training, but do not need to know  $L$  for testing. Hence, to train SAR-DRN and Ma2019,  $2.2 \times 10^4$  speckle-free optical images with single channel from ImageNet [25] are used as the ground-truth images, and the input speckled images can be obtained by adding speckle to the ground truth images according to (1) and (2). To make a fair comparison, the number of looks  $L$  is also randomly set to be 1, 2, 4, 8, and 16. Other parameters in SAR-DRN and Ma2019 are set as suggested in [15] and [16], respectively.

#### B. Performance Comparison on Synthetic Speckled Data

In this experiment, 100 optical remote sensing images (selected from Aerial Image data set (AID) [26]) are used for analyzing. To verify the despeckling effectiveness with the known noise level, the number of looks  $L$  of these images is set as 1, 4, and 16. Since the clean ground-truth images are available, the indices of peak signal to noise ratio (PSNR) and structural similarity index (SSIM) [27] are used for evaluation, and the comparison results are given in Table I. Chen2014 is performed following [10], as despeckling for 16-look images is not provided in [10]; to make a fair comparison, we only compare the despeckling results on one- and four-look images with Chen2014. As can be seen from Table I, our proposed methods outperform other methods in all noise levels. Moreover, the PSDi method can further improve the despeckling performance compared with the PSD method. Here, the highest SSIM values obtained by the proposed methods indicate the best structural features preservation, which can be beneficial for the applications, such as change detection with SAR images [3]. As the visual comparison shown in Fig. 3, only our proposed methods can remove speckle effectively.

TABLE II  
PERFORMANCE COMPARISON IN TERMS OF ENL, EPD-ROA, TCR, AND MoR ON REAL SAR DATA

Data	ENL		EPD-ROA		TCR		MoR	
	R1	R2	R3	R4	R5	R6	R1	R2
Original	12.40	4.61	-	-	-	-	-	-
Chen2014	66.78	104.26	0.8914	0.8404	1.3054	0.7723	0.9793	0.9736
SAR-BM3D	138.72	87.17	0.8917	0.8546	1.1303	0.7707	0.9590	0.9417
SAR-DRN	79.34	52.18	0.8928	0.8526	0.3370	0.4880	1.0305	1.0569
Ma2019	81.28	69.88	0.8931	0.8524	0.3332	0.6070	0.9484	0.9529
PSD	203.45	134.92	0.8980	0.8547	0.2356	<b>0.3651</b>	<b>1.0152</b>	<b>1.0109</b>
PSDi	<b>259.71</b>	<b>161.98</b>	<b>0.9018</b>	<b>0.8564</b>	<b>0.2348</b>	0.3945	1.0196	1.0122

#### C. Performance comparison on real SAR data

We also conduct despeckling experiments on real SAR data, where a three-look Ku-band miniSAR<sup>1</sup> image and a one-look C-band Sentinel-1 image are employed for evaluation. These images are cropped to  $512 \times 512$  pixels and  $320 \times 320$  pixels, respectively. The results are given in Fig. 4. Equivalent number of looks (ENL) [11], edge-preservation degree based on the ratio of average (EPD-ROA) [28], target-to-clutter ratio (TCR) [29], and mean of ratio (MoR) [11] are used as performance metrics to evaluate the degree of speckle reduction, edge preservation, point target preservation, and radiometric preservation, respectively [29]. The results are given in Table II.

As can be seen from Table II, SAR-BM3D and our proposed methods show better performance on speckle suppression. However, SAR-BM3D cannot show comparable performance as the proposed methods in preserving point target and radiometric. SAR-DRN and Ma2019 are trained based on supervised learning by using optical images and corresponding

<sup>1</sup>Courtesy of Sandia National Laboratories, Radar ISR.



TABLE III  
TIME CONSUMPTION COMPARISON ON IMAGES WITH 256×256 PIXELS

Chen2014	SAR-BM3D	SAR-DRN	Ma2019	PSD	PSDi
6.81s	18.42s	1.40s	<b>0.87s</b>	2.20s	2.21s

synthetic speckled images, which are quite different from real SAR images. This leads to the domain gap problem, which makes networks performed well on the data (i.e., synthetic images) in the same domain as the training data, but poorly performed on real data. This can be observed from the comparison results from Table I and Table II, i.e., SAR-DRN and Ma2019 cannot show high speckle suppression ability on real SAR images as that on synthetic speckled images. In contrast, it is worth noting that our proposed methods can learn despeckling by training the network on real SAR data. Hence, our proposed methods can achieve better despeckling performance on both synthetic speckled data and real SAR data. Meanwhile, our proposed methods show well features preservation ability. Especially, the proposed methods can obtain well tradeoff between EPD-ROA and ENL, which can be beneficial to agricultural area classification [1] and wetland classification [2].

In addition, we report the CPU time consumption of each method with the same system configuration, and the results are listed in Table III. Similar to other deep learning-based despeckling methods (i.e., SAR-DRN and Ma2019), once the networks are well trained, the despeckling process for a given SAR image is very quick. Our proposed methods have achieved superior despeckling performance with comparable time consumption, compared with SAR-DRN and Ma2019.

#### IV. CONCLUSION

We presented a practical deep learning-based methods for SAR image despeckling, which can achieve despeckling with only single speckled SAR images. Experiments conducted on both synthetic speckled data and real SAR data demonstrated the superiority of our methods compared with state-of-the-art methods. In our future study, we will explore the impact of speckle reduction and SAR feature preservation on applications using SAR images.

#### REFERENCES

- [1] V. Lukin *et al.*, “Despeckling of multitemporal sentinel SAR images and its impact on agricultural area classification,” in *Recent Advances and Applications in Remote Sensing*, London, U.K.: IntechOpen, 2018, pp. 3712–3719.
- [2] M. Mahdianpari, B. Salehi, and F. Mohammadimanesh, “The effect of PolSAR image despeckling on wetland classification: Introducing a new adaptive method,” *Can. J. Remote Sens.*, vol. 43, no. 5, pp. 485–503, Sep. 2017.
- [3] R. Wang, J.-W. Chen, L. Jiao, and M. Wang, “How can despeckling and structural features benefit to change detection on bitemporal SAR images?” *Remote Sens.*, vol. 11, no. 4, p. 421, Feb. 2019.
- [4] J.-S. Lee, “Digital image enhancement and noise filtering by use of local statistics,” *IEEE Trans. Pattern Anal. Mach. Intell.*, vol. PAMI-2, no. 2, pp. 165–168, Mar. 1980.
- [5] D. T. Kuan, A. A. Sawchuk, T. C. Strand, and P. Chavel, “Adaptive noise smoothing filter for images with signal-dependent noise,” *IEEE Trans. Pattern Anal. Mach. Intell.*, vol. PAMI-7, no. 2, pp. 165–177, Mar. 1985.

- [6] S. G. Chang, B. Yu, and M. Vetterli, “Adaptive wavelet thresholding for image denoising and compression,” *IEEE Trans. Image Process.*, vol. 9, no. 9, pp. 1532–1546, Sep. 2000.
- [7] H.-C. Li, W. Hong, Y.-R. Wu, and P.-Z. Fan, “Bayesian wavelet shrinkage with heterogeneity-adaptive threshold for SAR image despeckling based on generalized gamma distribution,” *IEEE Trans. Geosci. Remote Sens.*, vol. 51, no. 4, pp. 2388–2402, Apr. 2013.
- [8] G. Aubert and J.-F. Aujol, “A variational approach to removing multiplicative noise,” *SIAM J. Appl. Math.*, vol. 68, no. 4, pp. 925–946, Jan. 2008.
- [9] J. Shi and S. Osher, “A nonlinear inverse scale space method for a convex multiplicative noise model,” *SIAM J. Appl. Math.*, vol. 1, no. 3, pp. 294–321, Jan. 2008.
- [10] Y. Chen, W. Feng, R. Ranftl, H. Qiao, , and T. Pock, “A higher-order MRF based variational model for multiplicative noise reduction,” *IEEE Signal Process. Lett.*, vol. 21, no. 11, pp. 1370–1374, Nov. 2014.
- [11] S. Parrilli, M. Poderico, C. V. Angelino, , and L. Verdoliva, “A nonlocal SAR image denoising algorithm based on LMMSE wavelet shrinkage,” *IEEE Trans. Geosci. Remote Sens.*, vol. 50, no. 2, pp. 606–616, Feb. 2012.
- [12] F. Argenti, A. Lapini, T. Bianchi, and L. Alparone, “A tutorial on speckle reduction in synthetic aperture radar images,” *IEEE Geosci. Remote Sens. Mag.*, vol. 1, no. 3, pp. 6–35, Sep. 2013.
- [13] G. Chierchia, D. Cozzolino, G. Poggi, and L. Verdoliva, “SAR image despeckling through convolutional neural networks,” in *Proc. IEEE Int. Geosci. Remote Sens. Symp. (IGARSS)*, Jul. 2017, pp. 5438–5441.
- [14] P. Wang, H. Zhang, and V. M. Patel, “SAR image despeckling using a convolutional neural network,” *IEEE Signal Process. Lett.*, vol. 24, no. 12, pp. 1763–1767, Dec. 2017.
- [15] Q. Zhang, Q. Yuan, J. Li, Z. Yang, and X. Ma, “Learning a dilated residual network for SAR image despeckling,” *Remote Sens.*, vol. 10, no. 2, p. 196, Jan. 2018.
- [16] D. Ma, X. Zhang, X. Tang, J. Ming, and J. Shi, “A CNN-based method for SAR image despeckling,” in *Proc. IEEE Int. Geosci. Remote Sens. Symp. (IGARSS)*, Jul. 2019, pp. 4272–4275.
- [17] G. D. Martino, M. Poderico, G. Poggi, D. Riccio, and L. Verdoliva, “Benchmarking framework for SAR despeckling,” *IEEE Trans. Geosci. Remote Sens.*, vol. 52, no. 3, pp. 1596–1615, Mar. 2014.
- [18] J. Lehtinen *et al.*, “Noise2Noise: Learning image restoration without clean data,” in *Proc. Int. Conf. Mach. Learn.*, 2018, pp. 2965–2974.
- [19] Z. Zhou, M. Siddiquee, N. Tajbakhsh, and J. Liang, “UNet++: A nested U-Net architecture for medical image segmentation,” in *Proc. Int. Workshop Deep Learn. Med. Image Anal. Int. Workshop Multimodal Learn. Clin. Decis. Support*, 2018, pp. 3–11.
- [20] S. Cha, T. Park, and T. Moon, “GAN2GAN: Generative noise learning for blind image denoising with single noisy images,” *arXiv:1905.10488*, 2019. [Online]. Available: <http://arxiv.org/abs/1905.10488>
- [21] M. Arjovsky, S. Chintala, and L. Bottou, “Wasserstein generative adversarial networks,” in *Proc. 34th Int. Conf. Mach. Learn.*, 2017, pp. 214–223.
- [22] K. Zhang, W. Zuo, Y. Chen, D. Meng, and L. Zhang, “Beyond a gaussian denoiser: Residual learning of deep CNN for image denoising,” *IEEE Trans. Image Process.*, vol. 26, no. 7, pp. 3142–3155, Jul. 2017.
- [23] J.-Y. Zhu, T. Park, P. Isola, and A. A. Efros, “Unpaired image-to-image translation using cycle-consistent adversarial networks,” in *Proc. IEEE Int. Conf. Comput. Vis. (ICCV)*, Oct. 2017, pp. 2223–2232.
- [24] B. Lim, S. Son, H. Kim, S. Nah, , and K. M. Lee, “Enhanced deep residual networks for single image super-resolution,” in *Proc. IEEE Int. Conf. Comput. Vis. Pattern Recognit. Workshop (CVPRW)*, Jul. 2017, pp. 1132–1140.
- [25] O. Russakovsky *et al.*, “ImageNet large scale visual recognition challenge,” *Int. J. Comput. Vis.*, vol. 115, no. 3, pp. 211–252, Dec. 2015.
- [26] G.-S. Xia *et al.*, “AID: A benchmark data set for performance evaluation of aerial scene classification,” *IEEE Trans. Geosci. Remote Sens.*, vol. 55, no. 7, pp. 3965–3981, Jul. 2017.
- [27] Z. Wang, A. C. Bovik, H. R. Sheikh, and E. P. Simoncelli, “Image quality assessment: From error visibility to structural similarity,” *IEEE Trans. on Image Process.*, vol. 13, no. 4, pp. 600–612, Apr. 2004.
- [28] H. Feng, B. Hou, and M. Gong, “SAR image despeckling based on local homogeneous-region segmentation by using pixel-relativity measurement,” *IEEE Trans. Geosci. Remote Sens.*, vol. 7, no. 49, pp. 2724–2737, Jul. 2011.
- [29] X. Ma, P. Wu, Y. Wu, and H. Shen, “A review on recent developments in fully polarimetric SAR image despeckling,” *IEEE J. Sel. Top. Appl. Earth Obs. Remote Sens.*, vol. 11, no. 3, pp. 743–758, Mar. 2018.